

Supplementary material for the paper entitled:

Impact of buildings on surface solar radiation over urban Beijing

B. Zhao¹, K. N. Liou¹, Y. Gu¹, C. He¹, W. L. Lee², X. Chang³, Q. B. Li¹, S. X. Wang^{3, 4}, H. R. Tseng¹, L. R. Leung⁵, J. M. Hao^{3, 4}

[1] Joint Institute for Regional Earth System Science and Engineering and Department of Atmospheric and Oceanic Sciences, University of California, Los Angeles, CA 90095, USA

[2] Research Center for Environmental Changes, Academia Sinica, Taipei, Taiwan

[3] State Key Joint Laboratory of Environment Simulation and Pollution Control, School of Environment, Tsinghua University, Beijing 100084, China

[4] State Environmental Protection Key Laboratory of Sources and Control of Air Pollution Complex, Beijing 100084, China

[5] Pacific Northwest National Laboratory, Richland, WA 99352, USA

Correspondence to: B. Zhao [zhaob1206@gmail.com]

1 Evaluation of compatibility of the 3-D radiation parameterization associated with spatial resolutions

We evaluate the compatibility of the 3-D radiation parameterization associated with spatial resolutions. We first calculate surface solar flux deviations from the horizontal surface in each $4 \times 4 \text{ km}^2$ grid and $800 \times 800 \text{ m}^2$ grid with the 3-D radiation parameterization. Then, we compare flux deviations in each $4 \times 4 \text{ km}^2$ grid and the summation of all $800 \times 800 \text{ m}^2$ grids within the former. We select four $4 \times 4 \text{ km}^2$ grids (marked by red dashed rectangle in Fig. 1) to perform this evaluation, which exactly correspond to the whole Domain 2. The evaluation is performed for daily average flux deviations on April 1st and hourly flux deviations at selected times (7:00, 12:00, and 17:00 BT). The simulation results are summarized in Table S1. Here Grids 1, 2, 3, and 4 represent the upper-left, upper-right, lower-left, and lower-right grids, respectively.

Table S1 shows that biases between flux deviations calculated directly from 4 km grids and those from the summation of 800 m grids are within $\pm 0.025 \text{ W m}^{-2}$ for all grids and simulation periods, illustrating a reasonable compatibility between different grid resolutions.

2 Configuration of the WRF/CMAQ modelling system

For WRF/CMAQ simulations, we apply one-way, triple nesting domains, as shown in Fig. S1. Domain 1 covers China and part of East Asia and Southeast Asia at a grid resolution of $36 \text{ km} \times 36 \text{ km}$; Domain 2 covers the eastern China at a grid resolution of $12 \text{ km} \times 12 \text{ km}$; Domain 3 covers the provinces of Beijing, Tianjin, and Hebei at a grid resolution of $4 \text{ km} \times 4 \text{ km}$. We note that Domain 1 used in 3-D radiative transfer calculations is a part of Domain 3 that was used in WRF/CMAQ simulations, as illustrated in Fig. S1. CMAQ is configured using the AERO6 aerosol module and the CB-05 gas-phase chemical mechanism. WRFv3.3 is used to generate meteorological fields. The National Center for Environmental Prediction (NCEP)'s Final Operational Global Analysis data are used to generate the first guess field with a horizontal resolution of $1^\circ \times 1^\circ$ at every 6 h. The NCEP's Automated Data Processing (ADP) data are used in the objective analysis scheme. The physics options selected in the WRF model are the Kain Fritsch cumulus schemes, the Pleim-Xiu land surface model, the Pleim-Xiu planetary boundary layer scheme, the Morrison double-moment scheme for cloud microphysics, and the Rapid Radiative Transfer Model (RRTM) longwave and shortwave radiation scheme. We note that surface albedo is determined as a function of surface type, soil moisture, and solar zenith angle in the Pleim-Xiu land surface model (Pleim and Xiu, 1995). The Meteorology-Chemistry Interface Processor (MCIP) version 3.6 is applied to process meteorological data into a format required by CMAQ. The geographical projection, the vertical resolution, and the initial and boundary conditions of WRF/CMAQ are consistent with our previous papers (Zhao et al., 2013a; Zhao et al., 2015).

A high-resolution anthropogenic emission inventory for the Beijing-Tianjin-Hebei region developed by Tsinghua University is used (unpublished). Briefly, emissions are calculated at city levels and then distributed into $4 \times 4 \text{ km}^2$ grid cells using various spatial proxies at a resolution of $1 \times 1 \text{ km}^2$ using the methodology described in Streets et al. (2003). A unit-based method is applied to estimate emissions from large point sources including coal-fired power plants, iron and steel plants, and cement plants (Lei et al., 2011; Zhao et al., 2008). Anthropogenic emissions for other regions in China are developed by Zhao et al. (2013a, b) and Wang et al. (2014) for 2010, and subsequently updated to 2012 considering changes of

activity data and air pollution control technologies. Emissions for other Asian countries are compiled in the model inter-comparison program for Asia (MICS-Asia) phase III from a number of emission inventories. Biogenic emissions are calculated by the Model of Emissions of Gases and Aerosols from Nature (MEGAN, Guenther et al., 2006). The simulation periods include January, April, July, and October, 2012, representing four seasons.

3 Evaluation of meteorological and chemical simulations

3.1 Evaluation of meteorological variables

In this study, meteorological parameters simulated by WRFv3.3 are compared with observations obtained from the National Climatic Data Center (NCDC, <http://www.ncdc.noaa.gov/>), where hourly or every third hour observations are available for 28 sites scattered within Domain 3 used in WRF/CMAQ simulation (Fig. S1). Due to limited observational data available, statistical evaluation is restricted to temperature at 2 m, wind speed and wind direction at 10 m, and humidity at 2 m. The statistical indices used include the mean observation (Mean OBS), mean simulation (Mean SIM), bias, and gross error (GE). A detailed explanation of these indices can be found in Emery et al. (2001).

Table S2 lists the model performance statistics and benchmarks suggested by Emery et al. (2001). These benchmark values were derived based on performance statistics of the Fifth-Generation NCAR/Penn State Mesoscale Model (MM5) from a number of studies over the U.S. domain (mostly at grid resolutions of 12km or 4km), and have been widely accepted in many regional air quality modeling studies. We expect these standards should also be applicable in this study, considering that similar models (MM5 vs WRF) and grid resolutions are applied. For the wind speed and humidity, all statistical indices are within the benchmark range. For the temperature, in April, the bias and GE exceed the benchmark of ± 0.5 K and 2 K. Nevertheless, statistical indices for January, July, and October are within the benchmark range, indicating an acceptable performance. In summary, these statistics indicate an overall satisfactory performance of meteorological predictions.

3.2 Evaluation of fine particle (PM_{2.5}) simulation

The observational data of PM_{2.5} and its chemical components are quite sparse and not publicly available during simulation periods (January, April, July, and October, 2012). In order to evaluate the model performance in simulating fine particles, we conduct extra simulations for a field campaign period (from July 22nd to August 23rd, 2013) and compare simulated

concentrations $\text{PM}_{2.5}$ and its major chemical components with observations at two sites (unpublished data of Peking University and Tsinghua University), as shown in Fig. S2. Simulated $\text{PM}_{2.5}$ concentrations agree fairly well with observations; normalized mean biases (NMBs) are within $\pm 12\%$ for both sites. As for chemical components, NO_3^- concentration is overestimated (NMB = 79% to 95%), while SO_4^{2-} concentration is underestimated (NMB = -52% to -57%). There is a good agreement for NH_4^+ (NMB within $\pm 14\%$) and total SNA (Sulphate-nitrate-ammonium, NMB within $\pm 15\%$). The overestimation of NO_3^- and underestimation for SO_4^{2-} are consistent with previous studies over East Asia, probably attributed to the lack of some chemical formation pathways in the modeling system (Wang et al., 2011; Wang et al., 2013; Gao et al., 2014). As the mass extinction coefficients for NO_3^- , SO_4^{2-} , and NH_4^+ are quite similar, overestimation in NO_3^- and underestimation in SO_4^{2-} has limited effect on simulated aerosol optical depth (AOD), which serves as input for the FLG radiative transfer scheme. Simulated elemental carbon (EC) concentrations approximately double observed EC concentrations. EC concentrations are strongly affected by local emissions, while the spatial distribution of our emission inventory may not be able to capture local emission sources surrounding observational sites, leading to model-observation bias. The overestimation may also be attributable to the absence of EC aging in CMAQ, which leads to reduced fraction of hydrophilic EC and thus reduced wet deposition. Finally, concentrations of organic carbon (OC) are underestimated due to the underestimation of secondary organic aerosol (SOA) formation, which has been a common problem for widely-used chemical transport models (Carlton et al., 2010; Hallquist et al., 2009).

References

- Carlton, A. G., Bhawe, P. V., Napelenok, S. L., Edney, E. D., Sarwar, G., Pinder, R. W., Pouliot, G. A., and Houyoux, M.: Model representation of secondary organic aerosol in cmaq4.7, *Environ Sci Technol*, 44, 8553-8560, DOI 10.1021/Es100636q, 2010.
- Enhanced meteorological modeling and performance evaluation for two texas episodes. Report to the texas natural resources conservation commission[r/ol]: <http://www.tceq.state.tx.us/assets/public/implementation/air/am/contracts/reports/mm/EnhancedMetModelingAndPerformanceEvaluation.pdf>, access: 2015-03-01, 2001.
- Gao, Y., Zhao, C., Liu, X. H., Zhang, M. G., and Leung, L. R.: Wrf-chem simulations of aerosols and anthropogenic aerosol radiative forcing in east asia, *Atmos Environ*, 92, 250-266, DOI 10.1016/j.atmosenv.2014.04.038, 2014.

- 1 Guenther, A., Karl, T., Harley, P., Wiedinmyer, C., Palmer, P. I., and Geron, C.: Estimates of
2 global terrestrial isoprene emissions using megan (model of emissions of gases and aerosols
3 from nature), *Atmos Chem Phys*, 6, 3181-3210, 2006.
- 4 Hallquist, M., Wenger, J. C., Baltensperger, U., Rudich, Y., Simpson, D., Claeys, M.,
5 Dommen, J., Donahue, N. M., George, C., Goldstein, A. H., Hamilton, J. F., Herrmann, H.,
6 Hoffmann, T., Iinuma, Y., Jang, M., Jenkin, M. E., Jimenez, J. L., Kiendler-Scharr, A.,
7 Maenhaut, W., McFiggans, G., Mentel, T. F., Monod, A., Prevot, A. S. H., Seinfeld, J. H.,
8 Surratt, J. D., Szmigielski, R., and Wildt, J.: The formation, properties and impact of
9 secondary organic aerosol: Current and emerging issues, *Atmos Chem Phys*, 9, 5155-5236,
10 2009.
- 11 Lei, Y., Zhang, Q. A., Nielsen, C., and He, K. B.: An inventory of primary air pollutants and
12 co(2) emissions from cement production in china, 1990-2020, *Atmos Environ*, 45, 147-154,
13 doi: 10.1016/j.atmosenv.2010.09.034, 2011.
- 14 Pleim, J. E., and Xiu, A.: Development and testing of a surface flux and planetary boundary
15 layer model for application in mesoscale models, *J Appl Meteorol*, 34, 16-32, 1995.
- 16 Streets, D. G., Bond, T. C., Carmichael, G. R., Fernandes, S. D., Fu, Q., He, D., Klimont, Z.,
17 Nelson, S. M., Tsai, N. Y., Wang, M. Q., Woo, J. H., and Yarber, K. F.: An inventory of
18 gaseous and primary aerosol emissions in asia in the year 2000, *J Geophys Res-Atmos*, 108,
19 D21, doi: 10.1029/2002jd003093, 2003.
- 20 Wang, S. X., Xing, J., Chatani, S., Hao, J. M., Klimont, Z., Cofala, J., and Amann, M.:
21 Verification of anthropogenic emissions of china by satellite and ground observations,
22 *Atmos Environ*, 45, 6347-6358, DOI 10.1016/j.atmosenv.2011.08.054, 2011.
- 23 Wang, S. X., Zhao, B., Cai, S. Y., Klimont, Z., Nielsen, C. P., Morikawa, T., Woo, J. H., Kim,
24 Y., Fu, X., Xu, J. Y., Hao, J. M., and He, K. B.: Emission trends and mitigation options for
25 air pollutants in east asia, *Atmos Chem Phys*, 14, 6571-6603, DOI 10.5194/acp-14-6571-
26 2014, 2014.
- 27 Wang, Y., Zhang, Q. Q., He, K., Zhang, Q., and Chai, L.: Sulfate-nitrate-ammonium aerosols
28 over china: Response to 2000-2015 emission changes of sulfur dioxide, nitrogen oxides,
29 and ammonia, *Atmos Chem Phys*, 13, 2635-2652, DOI 10.5194/acp-13-2635-2013, 2013.
- 30 Zhao, B., Wang, S. X., Wang, J. D., Fu, J. S., Liu, T. H., Xu, J. Y., Fu, X., and Hao, J. M.:
31 Impact of national nox and so2 control policies on particulate matter pollution in china,
32 *Atmos Environ*, 77, 453-463, DOI 10.1016/j.atmosenv.2013.05.012, 2013a.
- 33 Zhao, B., Wang, S. X., Liu, H., Xu, J. Y., Fu, K., Klimont, Z., Hao, J. M., He, K. B., Cofala,
34 J., and Amann, M.: NOx emissions in china: Historical trends and future perspectives,
35 *Atmos Chem Phys*, 13, 9869-9897, DOI 10.5194/acp-13-9869-2013, 2013b.
- 36 Zhao, B., Wang, S. X., Xing, J., Fu, K., Fu, J. S., Jang, C., Zhu, Y., Dong, X. Y., Gao, Y., Wu,
37 W. J., Wang, J. D., and Hao, J. M.: Assessing the nonlinear response of fine particles to
38 precursor emissions: Development and application of an extended response surface
39 modeling technique v1.0, *Geosci Model Dev*, 8, 115-128, DOI 10.5194/gmd-8-115-2015,
40 2015.
- 41 Zhao, Y., Wang, S. X., Duan, L., Lei, Y., Cao, P. F., and Hao, J. M.: Primary air pollutant
42 emissions of coal-fired power plants in china: Current status and future prediction, *Atmos*
43 *Environ*, 42, 8442-8452, DOI 10.1016/j.atmosenv.2008.08.021, 2008.
- 44
- 45

Tables and figures

Table S1. Comparison of surface solar flux deviations between the 3-D radiation parameterization and the plane-parallel scheme calculated directly from 4 km grids and from summation of 800 m grids (W m^{-2}).

	4 km	800 m	Bias (800 m – 4 km)	4 km	800 m	Bias (800 m – 4 km)
	Daily average			7:00		
4-grid average	0.103	0.100	-0.003	0.006	0.016	0.010
Grid 1	-0.071	-0.057	0.014	-0.329	-0.314	0.015
Grid 2	-0.018	-0.032	-0.014	0.055	0.058	0.003
Grid 3	0.394	0.387	-0.007	-0.230	-0.218	0.012
Grid 4	0.105	0.103	-0.002	0.528	0.539	0.011
	12:00			17:00		
4-grid average	0.502	0.499	-0.003	-0.895	-0.909	-0.014
Grid 1	0.173	0.198	0.025	-0.616	-0.627	-0.011
Grid 2	0.391	0.368	-0.023	-1.275	-1.289	-0.014
Grid 3	0.967	0.956	-0.011	-0.451	-0.469	-0.018
Grid 4	0.476	0.475	-0.001	-1.236	-1.252	-0.016

Table S2. Statistical results for the comparison of simulated meteorological parameters with NCDC observations.

	Wind speed (m s^{-1})				Temperature (K)				Humidity (g kg^{-1})			
	Mean OBS ^a	Mean SIM	Bias	GE	Mean OBS	Mean SIM	Bias	GE	Mean OBS	Mean SIM	Bias	GE
Benchmark			$\leq \pm 0.5$	≤ 2			$\leq \pm 0.5$	≤ 2			$\leq \pm 1$	≤ 2
Jan, 2012	2.34	2.59	0.24	1.12	266.1	266.2	0.13	1.64	1.23	1.36	0.13	0.29
Apr, 2012	3.39	3.65	0.27	1.42	287.4	286.0	-1.37	2.83	4.62	4.44	-0.18	0.85
Jul, 2012	2.32	2.51	0.20	1.08	298.0	297.8	-0.22	1.72	14.80	14.56	-0.23	1.53
Oct, 2012	2.38	2.69	0.32	1.19	285.0	285.6	0.61	1.52	4.87	4.54	-0.34	0.80

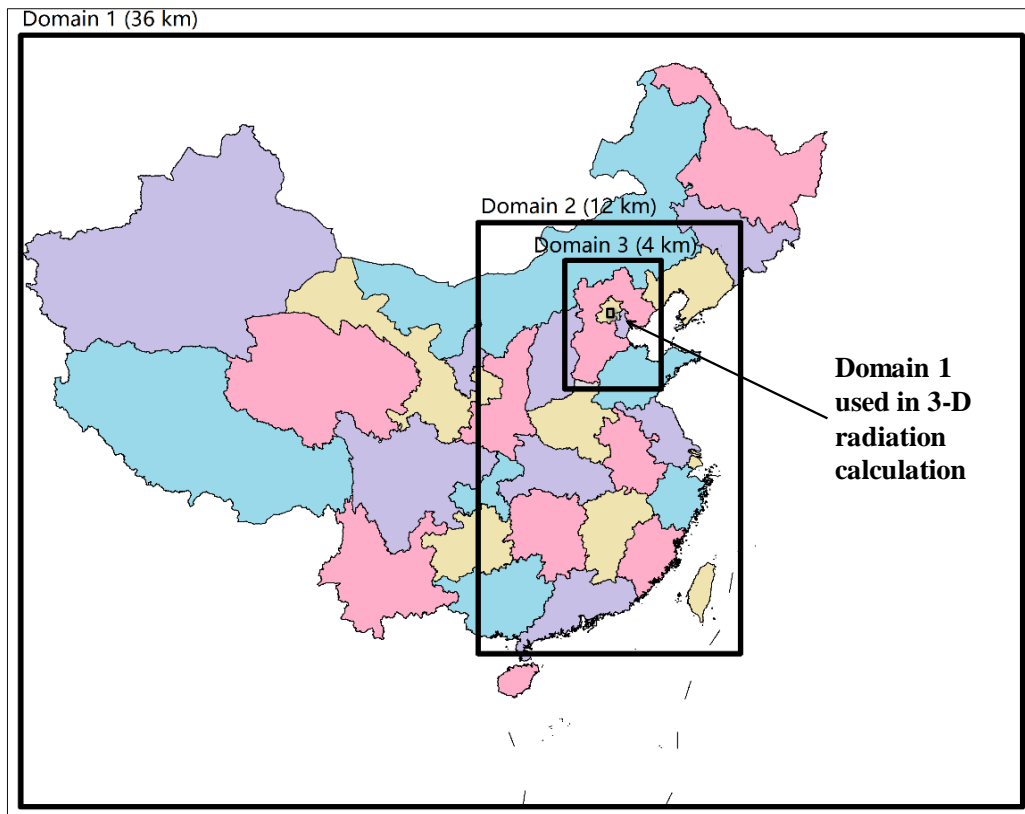
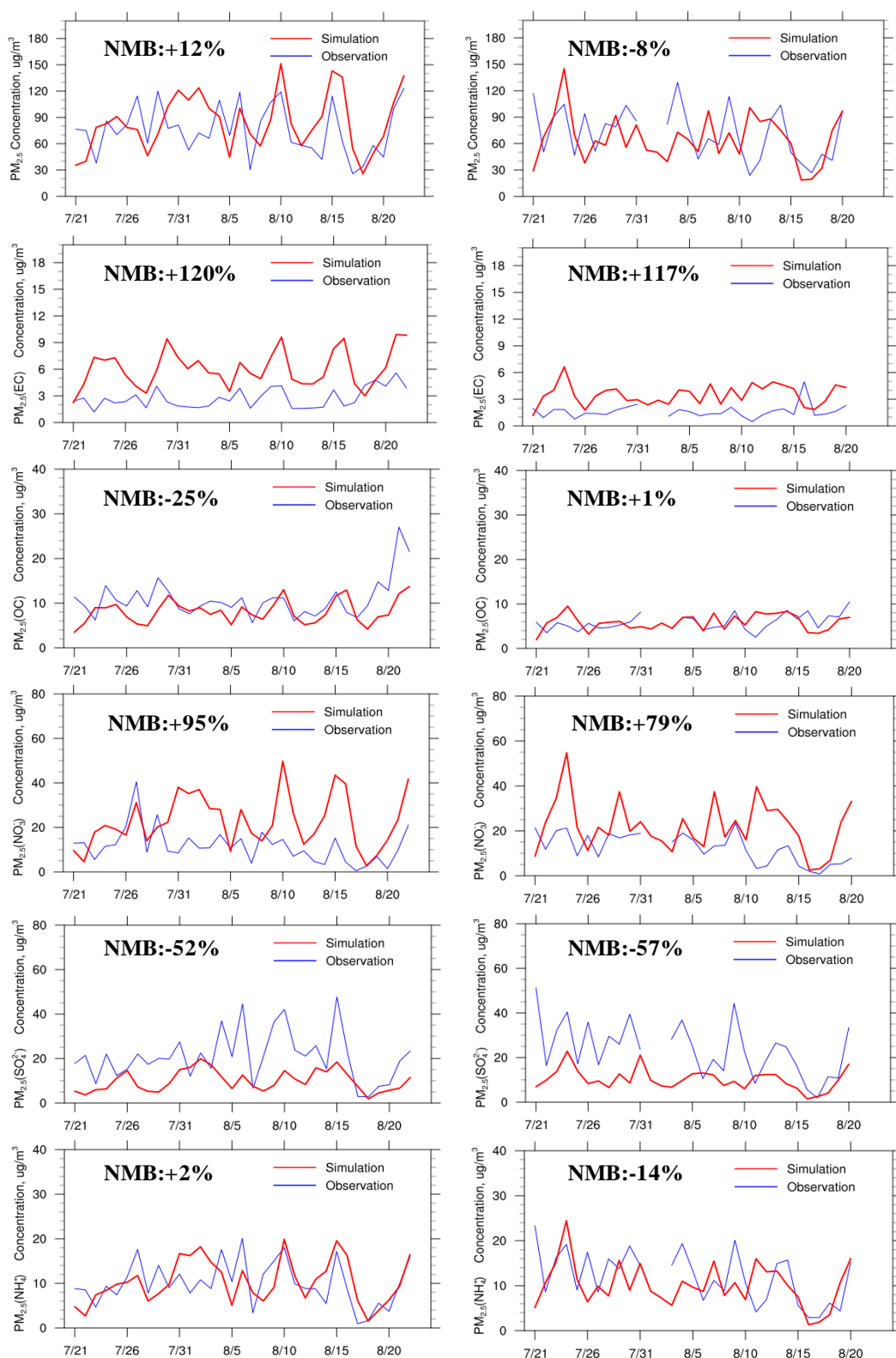
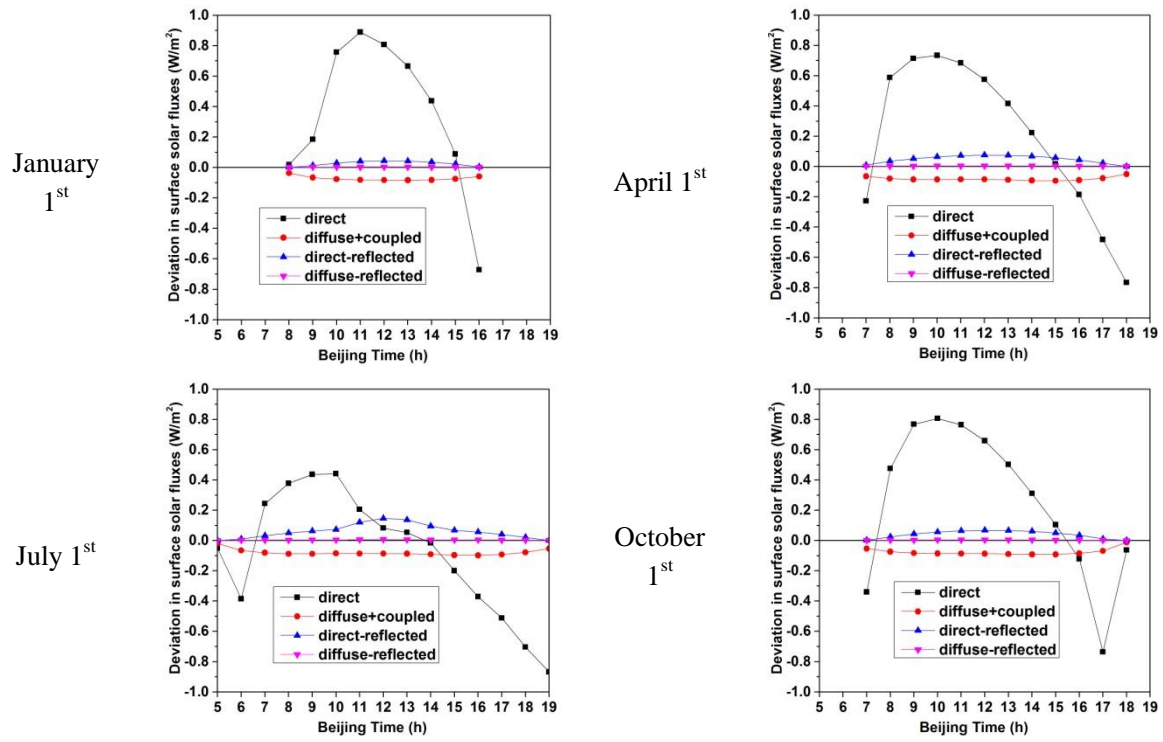


Figure S1. Triple nesting domains used in WRF/CMAQ simulation and illustration of Domain 1 used in 3-D radiative transfer calculation (defined in Fig. 1) against WRF/CMAQ domains. The colours represent different provinces/regions.



1
2 Figure S2. Comparison of simulated and observed concentrations of $PM_{2.5}$ and its major
3 chemical components at the Xiong County site (left) and the Ling County site (right). The
4 panels show model-observation comparison of total $PM_{2.5}$, EC, OC, NO_3^- , SO_4^{2-} , and NH_4^+
5 from top to bottom.



1 Figure S3. Contributions of individual components to surface solar flux deviations between
 2 the 3-D radiation parameterization and the plane-parallel scheme in clear-sky condition
 3 without aerosols in a typical urban area in Domain 1 (defined as Rectangle B in Fig. 1).